# Development of a Phoswich Detector for Alpha, Beta, and Gamma-Ray Emitting Radionuclide Identification for Decommissioning – 26170

Dai Tateishi[1], Yuta Terasaka[1], Yuki Morishita[1], and Yuki Sato[1]
[1] Collaborative Laboratories for Advanced Decommissioning Science (CLADS),
Japan Atomic Energy Agency

## ABSTRACT

To ensure the safe decommissioning of the Fukushima Daiichi Nuclear Power Station, we developed a spectrum analysis method for the phoswich detector that can identify alpha-, beta-, and gamma-ray-emitting radionuclides, even in the presence of high gamma-ray backgrounds. The detector uses ZnS(Ag) and plastic scintillators to distinguish radionuclides by energy spectrum analysis. Tests with $^{241}$Am, $^{90}$Sr, $^{57}$Co , $^{137}$Cs $(\beta+\gamma)$, $^{137}$Cs $(\gamma)$ revealed distinct spectral shapes and slopes, facilitating successful radionuclide identification of $^{241}$Am, $^{90}$Sr, $^{137}$Cs $(\beta)$, and $^{137}$Cs $(\gamma)$. However, we found no observable difference in the energy spectral shapes between $^{57}$Co and $^{137}$Cs gamma-ray emissions, which limited our spectral analysis method's ability to distinguish between these two radionuclides. This method improves upon previous smear-based techniques by detecting fixed contamination and differentiating between beta and gamma sources. The approach holds promise for applications in the characterization and treatment of radioactive waste.

## INTRODUCTION

To ensure the safe decommissioning of the Fukushima Daiichi Nuclear Power Station (FDNPS), it is essential to accurately estimate the distribution of radioactive contamination within the reactor buildings (R/B). Thus far, contamination from gamma-ray-emitting radionuclides—primarily responsible for external exposure—has been mapped using Compton cameras [1] and inverse estimation techniques [2]. However, the contamination distribution of alpha-emitting radionuclides, which contribute to internal exposure, and beta-emitting radionuclides, which pose risks to exposure to the lens of the eye [3], are not well understood. These nuclides have mainly been assessed through indirect methods using smear filter paper, which do not account for fixed contamination. Therefore, there is a need for radiation detectors capable of directly and simultaneously identifying multiple types of radiation, even in environments with high gamma-ray backgrounds.

One promising approach is the use of a phoswich detector, which consists of multiple scintillators with different light yield and decay time constants stacked together. A photodetector reads the scintillation light emitted from each layer, and the pulse shape analysis distinguishes the type of incident radiation. We developed a phoswich detector composed of a ZnS(Ag) scintillator for alpha-particle detection and a plastic scintillator for beta-particle detection. This configuration has successfully identified alpha- and beta-emitting radionuclides in smear filter samples collected from FDNPS [4] using conventional pulse shape discrimination analysis. However, this method lacked the resolution required for detailed nuclide identification, especially for beta- and gamma-ray-emitting radionuclides.

In this study, we focused on the possibility that the energy deposited to the scintillator differs between $^{137}$Cs and $^{90}$Sr. By evaluating the energy spectrum obtained in each measurement, we conceived a method to identify not only the type of ionizing radiation but also the specific radionuclides. The objective of this study is to evaluate the performance of this new method and assess its feasibility for use within the R/B of the FNDPS.

## MATERIALS AND METHODS

### Detector Design and Configuration

Figures 1 (a) and (b) show the schematic diagram and photograph of the phoswich detector we developed, respectively. The detector consists of two layers of scintillators, a multi-anode photomultiplier tube (MAPMT), and a data acquisition system. We stacked a 10 $mg/cm^2$ equivalent thickness of ZnS(Ag) scintillator for alpha-particle detection, and a 1.7 mm thick plastic scintillator for beta-particle detection, respectively. The scintillation light from these scintillators is detected by a position-sensitive MAPMT and output as four analog signals $(X+, X-, Y+, Y-)$. These analog signals are then converted into position and energy information for each event as they pass through an amplifier, analogue-to-digital converters (ADCs), and a field-programmable gate array (FPGA). This setup enables precise imaging and spectral analysis. See the reference [4] for the details of the data acquisition system.

The digitized data exported from the FPGA were transmitted via Ethernet cable to the laptop and stored. We used Python software called Data Acquisition for Phoswich Imaging Detector (DAPID) [4]-[12] for visualization and spectrum analysis, which was installed on the laptop.

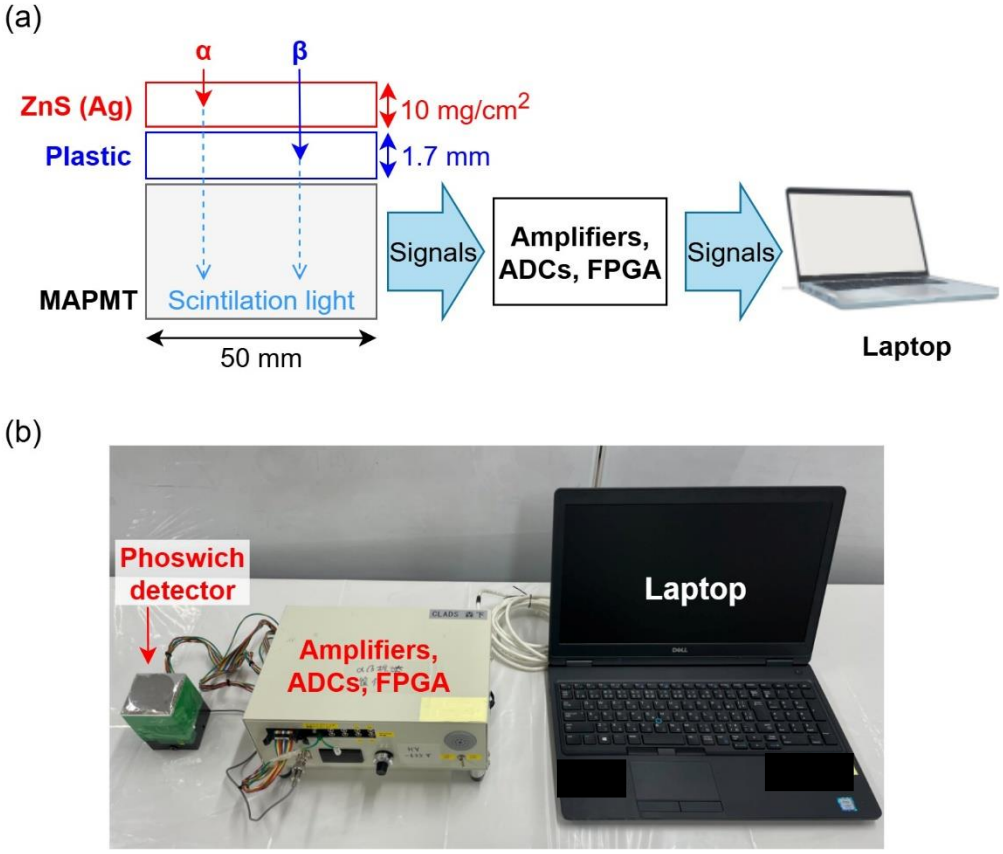


Figure 1. Schematic diagram and photograph of the detector. (a) A schematic image of our phoswich detector. (b) Photograph of the detector used for our measurement.

### Performance Evaluation Tests

To evaluate the energy spectrum of alpha, beta, and gamma-rays obtained with this detector, we placed 5 calibration sources ($^{241}$Am, $^{90}$Sr, $^{57}$Co, $^{137}$Cs $(\beta + \gamma)$, and $^{137}$Cs $(\gamma)$) in front of the detector, as shown

in Figure 2, and conducted 5-minute measurements. We selected $^{241}$Am, $^{90}$Sr, and $^{137}$Cs as nuclear fission products, and $^{57}$Co to represent the scattering component of gamma-rays from $^{137}$Cs. The details of the calibration sources are provided in Table 1. During the measurements, we varied the trigger voltage five times (206, 307, 409, 501, and 607 mV) and adjusted the trigger threshold to an optimal value, enabling the detection of all nuclides. Throughout the measurement, we set the high voltage of the PMT to -625 V.

To quantitatively evaluate waveforms of scintillation light, we calculated the total integral ($Z_{\mathrm{tot}}$) value—integrating each signal from peak to 640 ns—and the partial integral ($Z_{\mathrm{par}}$) value integrating each signal from peak up to 320 ns. We applied the following two analysis methods to compare the effectiveness of spectrum analysis.

1. Conventional method: Pulse shape discrimination
   This method focuses on the differing decay times of scintillation light in ZnS (Ag) and plastic scintillators. We regarded alpha-particle events as events with 45 ch $\leq Z_{\mathrm{tot}} \leq$ 127 ch and 30 ch $\leq Z_{\mathrm{par}} \leq$ 85 ch, and beta-particle events as events with 13 ch $\leq Z_{\mathrm{tot}} \leq$ 36 ch and 12 ch $\leq Z_{\mathrm{par}} \leq$ 36 ch, respectively.

2. Our new approach: Spectral analysis
   In our new method, we created the spectrum for each measurement by dividing the $Z_{\mathrm{tot}}$ into bins, with one channel per bin, spanning a range of 0 to 160 channels.

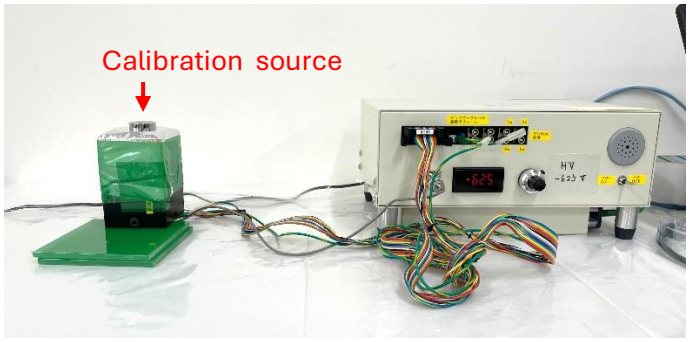


Figure 2. A photograph of the detectors during measurement.

Table 1. Calibration sources used in our experiment

| Radio isotope | Types of radiation | Shape | Radioactivity (2025/10/28) |
|---|---|---|---|
| $^{241}$Am | $\alpha$ | Plane | 3.11 kBq |
| $^{90}$Sr | $\beta$ | Plane | 2.4 kBq |
| $^{137}$Cs | $\beta + \gamma$ | Coin | 7.2 kBq |
| $^{137}$Cs | $\gamma$ | Coin | 7.2 kBq |
| $^{57}$Co | $\gamma$ | Cylinder | 1.9 MBq |

## RESULTS

### Conventional Method: Pulse Shape Discrimination

To verify the ability to distinguish radioactive isotopes, we created a $Z_{\mathrm{tot}}$ vs. $Z_{\mathrm{par}}$ distribution map. The resultant map of $^{241}$Am, $^{90}$Sr, $^{57}$Co, $^{137}$Cs $(\beta + \gamma)$, $^{137}$Cs $(\gamma)$, and background for trigger voltages of 206, 307, 409 mV, and 501, 607 mV are shown in Figures 3 and 4, respectively. The red and blue boxes in the figures represent the alpha- and beta- particle range, respectively.

### Our New Approach: Spectral Analysis

The resultant spectrum of $^{241}$Am, $^{90}$Sr, $^{57}$Co, $^{137}$Cs $(\beta + \gamma)$, $^{137}$Cs $(\gamma)$, and along with the background for trigger voltages of 206, 307, 409 mV, and 501, 607 mV are shown in Figures 5 and 6, respectively. In these figures, the blue, orange, green, red, purple, and black line represent the energy spectrum of $^{241}$Am, $^{90}$Sr, $^{57}$Co, $^{137}$Cs $(\beta + \gamma)$, $^{137}$Cs $(\gamma)$, and background, respectively.

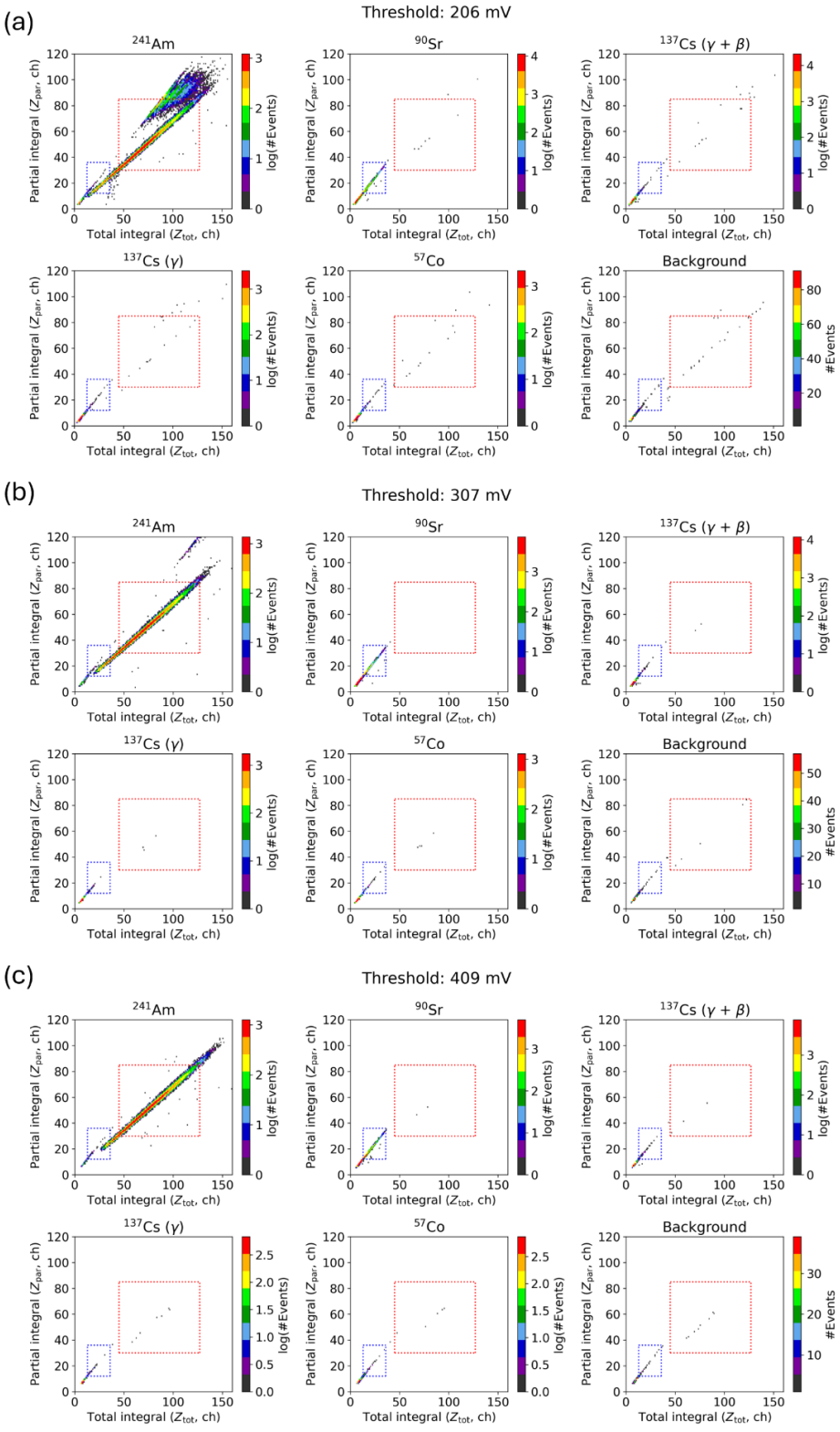


Figure 3. $Z_{\mathrm{tot}}$ vs. $Z_{\mathrm{par}}$ map of $^{241}$Am, $^{90}$Sr, $^{57}$Co, $^{137}$Cs ($\beta + \gamma$), $^{137}$Cs ($\gamma$), and background. (a), (b), and (c) represent the measurement result with trigger voltages of 206, 307, 409 mV, respectively. The red and blue box represents the alpha and beta particle range, respectively.

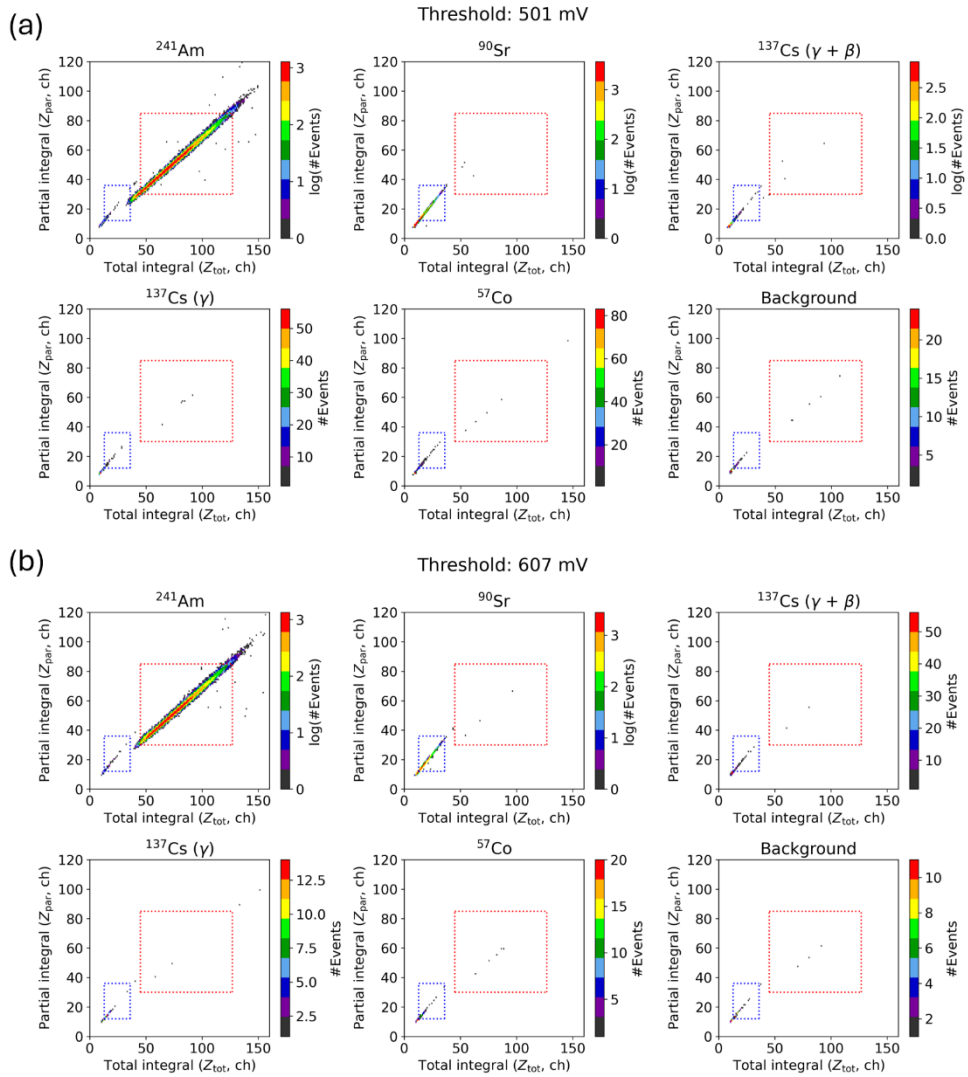


Figure 4. $Z_{\mathrm{tot}}$ vs. $Z_{\mathrm{par}}$ map of $^{241}$Am, $^{90}$Sr, $^{57}$Co, $^{137}$Cs ($\beta + \gamma$), $^{137}$Cs ($\gamma$), and background. (a) and (b) represent the measurement result with trigger voltages of 501 and 607 mV, respectively. The red and blue box represents the alpha and beta particle range, respectively.

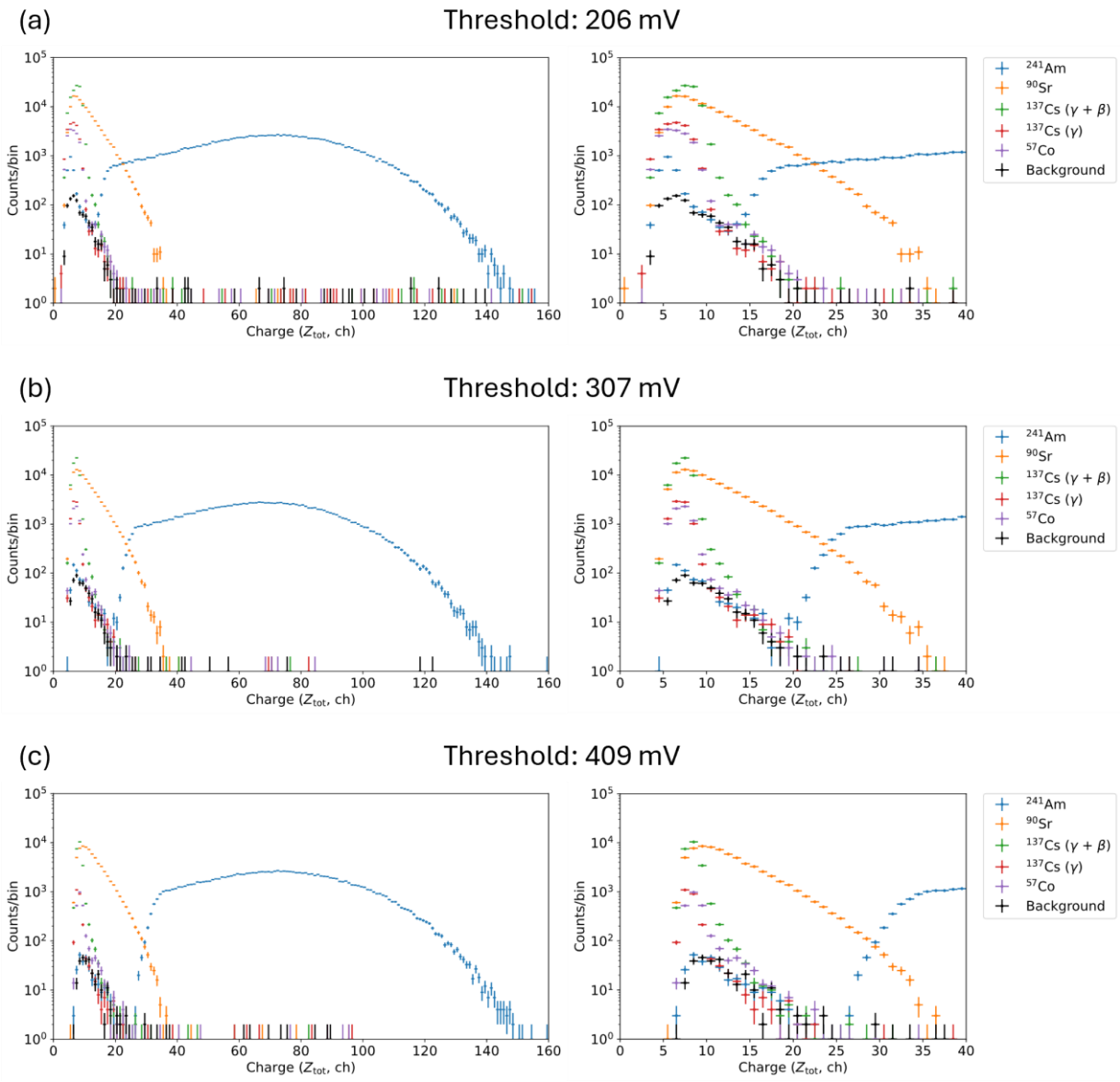


Figure 5. The spectrum of $^{241}$Am, $^{90}$Sr, $^{57}$Co, $^{137}$Cs $(\beta + \gamma)$, $^{137}$Cs $(\gamma)$, and background for trigger voltages of 206, 307, and 409 mV. The blue, orange, green, red, purple, and black line represent the spectrum of $^{241}$Am, $^{90}$Sr, $^{57}$Co, $^{137}$Cs $(\beta + \gamma)$, $^{137}$Cs $(\gamma)$, and background, respectively.

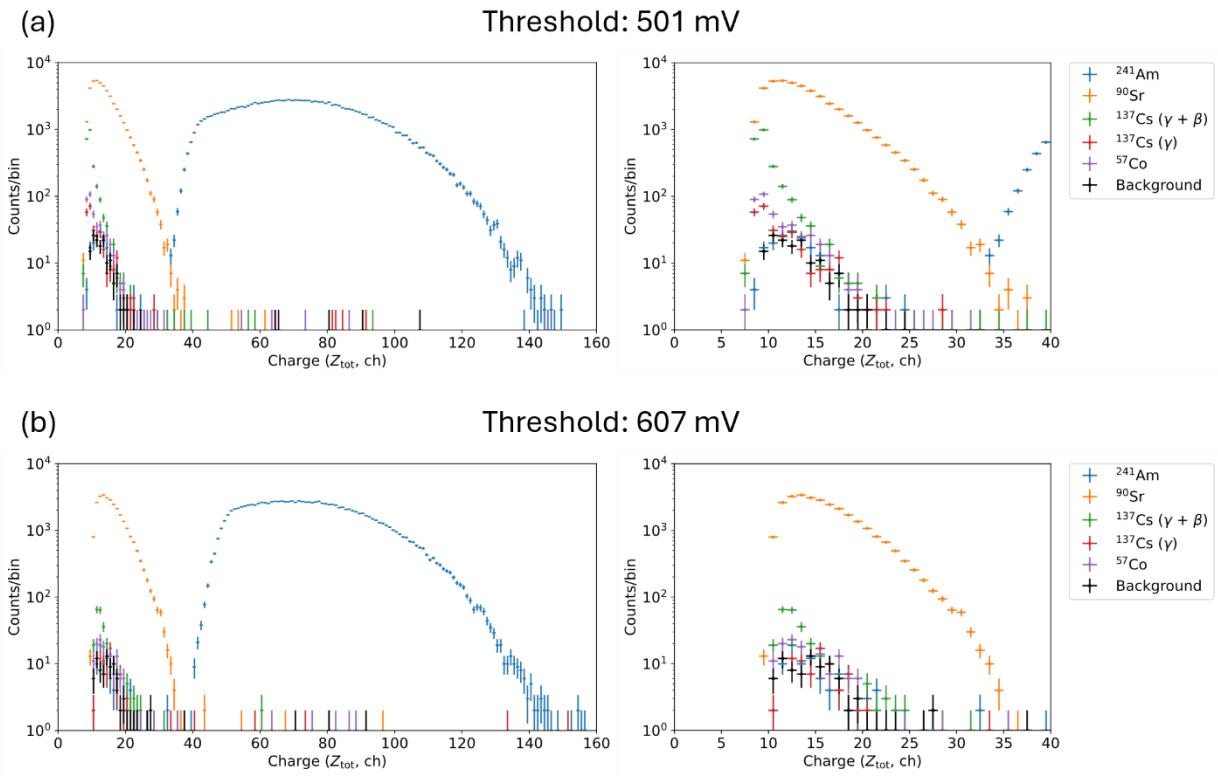


Figure 6. The spectrum of $^{241}$Am, $^{90}$Sr, $^{57}$Co, $^{137}$Cs $(\beta + \gamma)$, $^{137}$Cs $(\gamma)$, and background for trigger voltages of 501 and 607 mV. The blue, orange, green, red, purple, and black line represent the spectrum of $^{241}$Am, $^{90}$Sr, $^{57}$Co, $^{137}$Cs $(\beta + \gamma)$, $^{137}$Cs $(\gamma)$, and background, respectively.

## DISCUSSION

The energy spectrum presented in Figures 5 and 6 shows that the alpha-particle-emitting source produced a distinct peak, while the beta- and gamma-ray-emitting sources displayed a continuous spectrum. The energy spectrum for each beta- and gamma-ray-emitting radionuclide varied in terms of slope and shape. Additionally, we discovered that adjusting the trigger threshold affects the shape of the spectrum.

### Differences in Energy Spectrum When the Threshold Varies

As shown in Figures 5 and 6, the energy spectrum exhibited different responses for alpha particles and beta-gamma-rays when the trigger threshold was adjusted.

For alpha particles, lowering the threshold revealed a tail-like structure on the low-energy side. This phenomenon was unexpected, as we anticipated a Gaussian-like spectrum. This discrepancy is likely due to the opaque white appearance of ZnS (Ag), where the scintillation light is scattered by surrounding materials, leading to energy attenuation. Furthermore, when the trigger threshold was set to 206 mV, we observed a Gaussian-like structure peaking around 6 ch which could not be attributed to background components. This feature is considered to be the emission line from 59.5 keV gamma-rays emitted by $^{241}$Am.

Unlike alpha-particles, the spectrum shape for beta-particles and gamma-rays remain continuous, even when the trigger threshold is adjusted. Increasing the trigger threshold raises the peak value while lowering the overall spectrum height. This phenomenon can be explained qualitatively by the continuous

energy spectrum of beta-particles. At the energies of gamma-rays emitted by $^{137}$Cs and $^{57}$Co, Compton scattering becomes the primary interaction in plastic scintillators. Consequently, only a portion of the energy is deposited to the scintillator, leading to a continuous energy distribution.

**Radio Isotope Discrimination Capability and Optimal Threshold Values**

The discrimination capability to identify radioactive nuclides varies depending on the threshold values, as described below.

- $^{241}$Am, $^{90}$Sr, and $^{137}$Cs (both beta- and gamma-ray):
  Our spectral analysis enabled the identification of these nuclides at all thresholds. However, for $^{241}$Am and $^{90}$Sr, setting the threshold to 501 mV or lower resulted in overlap between the two nuclides in certain energy bands.

- $^{137}$Cs ($\beta$) and $^{137}$Cs ($\gamma$):
  Our spectral analysis can differentiate between these two effects by subtracting the $^{137}$Cs ($\gamma$) spectrum from the $^{137}$Cs ($\beta + \gamma$) spectrum at all thresholds.

- $^{137}$Cs ($\gamma$) and $^{57}$Co:
  The energy spectrum of both radioisotopes exhibited a similar spectrum at every threshold, and our method could not distinguish between them.

Based on the above measurement results, we determine that setting the threshold to ~400 - ~500 mV is appropriate to enable the identification of the largest number of radioisotopes through spectral analysis. Furthermore, in a high ambient gamma-ray dose rate environment, setting a higher threshold is expected to reduce the interference of the gamma-ray spectrum to the beta-particle spectrum of $^{90}$Sr. Future tests at the radiation irradiation facility involving gamma-ray irradiation from $^{137}$Cs are required to confirm how the gamma-ray spectrum responds to changes in the threshold.

**Comparison with Conventional Analysis Methods**

Figures 3 and 4 show the results obtained using the conventional analysis method. This technique demonstrated that setting the threshold to ~500 mV or higher enables discrimination between alpha- and beta-emitting-particles. However, gamma-ray-derived events were also present within the beta-particle identification region. Therefore, in environments with a gamma-ray background, beta-particle events may be overestimated.

In contrast to the conventional method, our spectral analysis may reduce this interference by fitting the observed spectrum with the model created from calibration source spectrum. Considering the above, we suggest that our spectral analysis is an effective method for measurements within the R/B of the FDNPS, where the gamma-ray background is high.

**Future Applications**

Our spectral analysis method enables the identification of radionuclides even in environments where gamma-rays are present. This result indicates that we will be able to use this detector for measurements inside the R/B of the FDNPS, enabling us to improve upon previous smear-based techniques by detecting fixed contamination and differentiating between beta- and gamma-ray sources. Additionally, this method

will also help estimate the radioactive isotopes contained in radioactive waste generated during future decommissioning activities.

## SUMMARY AND CONCLUSIONS

We developed a spectrum analysis method for the phoswich detector capable of identifying alpha, beta, and gamma-ray-emitting radionuclides, even in the presence of gamma-ray backgrounds. The detector utilizes ZnS(Ag) and plastic scintillators to distinguish radionuclides based on energy spectrum analysis.

In our performance tests, we measured the spectrum of several radionuclides: $^{241}$Am, $^{90}$Sr, $^{57}$Co, and $^{137}$Cs for both beta-gamma and gamma-ray only emissions. We found that the spectral shapes were distinct for $^{241}$Am, $^{90}$Sr, and $^{57}$Co, while $^{137}$Cs displayed notably different profiles for its beta-gamma and gamma emissions.

Additionally, we were able to estimate the contribution of beta-particle emissions of $^{137}$Cs by subtracting the gamma-ray spectrum of $^{137}$Cs from the beta-gamma spectrum. However, we found no observable difference in the energy spectral shapes between $^{57}$Co and $^{137}$Cs gamma-ray emissions, which limited our spectral analysis method's ability to distinguish between these two radionuclides.

Our method improves upon previous smear-based techniques by detecting fixed contamination and differentiating between beta and gamma sources. The approach holds promise for applications in the characterization and treatment of radioactive waste.

## REFERENCES

1. Y. Sato et al., “Detailed visualization of radioactive hotspots inside the unit 1 reactor building of the Fukushima Daiichi Nuclear Power Station using an integrated Radiation Imaging System mounted on a Mecanum wheel robot,” Journal of Nuclear Science and Technology, vol. 61, 2024, doi: 10.1080/00223131.2023.2282551
2. M. Machida et al., “R&D of digital technology on inverse estimation of radioactive source distributions and related source countermeasures; R&D status of digital platform including 3D-ADRES-indoor,” RIST News, vol. 68, pp.3-19, Sep. 2022 (in Japanese).
3. Y. Yokoyama et al., “Measurements of the doses of eye lens for the workers of Fukushima Daiichi Nuclear Power Plant,” Radiat. Meas. 138, Nov., 2020, doi: 10.1016/j.radmeas.2020.106399
4. Y. Morishita et al., “A phoswich alpha/beta detector for monitoring in the site of Fukushima Daiichi Nuclear Power Station,” Radiat. Meas. 160, Jan., 2023, doi: 10.1016/j.radmeas.2022.106896